20

Application of the Unscented Kalman Filter (UKF) Estimation Techniques for Fault Detection Diagnosis and Isolation (FDDI) in Attitude Control (AC) and Heating Ventilation Air Conditioning (HVAC) Systems

Nicolae Tudoroiu[1], Kash Khorasani[1], Mohammed Zaheeruddin[1], Eshan Sobhani-Tehrani[1], Dumitru Burdescu[2] and Elena-Roxana Tudoroiu[3]
[1]*Concordia University, Montreal,*
[2]*University of Craiova,*
[3]*West University Politehnica Timisoara,*
[1]*Canada*
[2,3]*Romania*

1. Introduction

In this work we investigate two main applications of the detection and isolation of partial (soft) and total (hard) failures in the reaction wheel (RW) actuators of the satellite attitude control systems (ACS) and in the Heating Ventilation and Air Conditioning (HVAC) valve actuators respectively. The fault detection diagnosis and isolation (FDDI) is accomplished using a probabilistic approach based on the interactive multiple models (IMM) schemes embedded with Extended Kalman Filter (EKF) or Unscented Kalman Filter (UKF) estimation techniques. Towards this objective, the healthy modes of the ACS and HVAC systems under different operating conditions as well as a number of different fault scenarios including changes and anomalies in the temperature, power supply bus voltage, and unexpected current variations in the actuators of each axis of the satellite, or leakage, stuck-open and stuck-close fault modes in the HVAC actuator valves are considered. We describe and develop a bank of interacting multiple model Extended Kalman Filters (IMM_EKF) or Unscented Kalman Filters (IMM_UKF) to detect and isolate the above mentioned reaction wheel and valve failures in the ACS and HVAC systems. Also, it should be emphasized that the proposed IMM_EKF and IMM_UKF techniques are implemented based on high-fidelity highly nonlinear models of a commercial ITHACO RWA and discharge air temperature (DAT) cooling or heating coils. Compared to other fault detection diagnosis and isolation (FDDI) strategies developed in the control systems literature, the proposed FDDI schemes is shown, through extensive numerical simulations by using MATLAB and SIMULINK software packages, to be more accurate, less computationally demanding, and more robust with the potential of extending to a number of other engineering applications. Also, the proposed algorithms deal directly with the nonlinear dynamics of the system, the

Source: Kalman Filter: Recent Advances and Applications, Book edited by: Victor M. Moreno and Alberto Pigazo,
ISBN 978-953-307-000-1, pp. 584, April 2009, I-Tech, Vienna, Austria

unanticipated valve actuator failures and statistic properties of the process noise and measurements such as the mean and covariance matrices in the most general formulation based on the Extended Kalman Filter (EKF) or Unscented Kalman Filter (UKF) estimation theory [Tudoroiu & Khorasani, 2007; Tudoroiu et al., 2006; Plett, 2004; Haykin 2003; Joseph, 2003; Wan & Merwe, 2000; Julier & Uhlman, 1997]. The satellite's attitude control system (ACS) faults caused by malfunctions in its components, actuators, and sensors result from unexpected interferences or gradual aging of system components. These faults could result in higher energy consumption, loss of the vehicle control, and in case of total failures catastrophic loss of the satellite. With increasing emphasis recently placed on energy efficiency and equipment safety and reliability, there is a need to develop robust intelligent and autonomous tools capable of detecting, isolating and diagnosing any sensor, actuator or system component fault so that remedial reconfiguration and recovery actions could be taken as soon as possible with minimal support from ground station and operators. The increasing complexity of space vehicles and the prevailing cost reduction measures have necessitated calls for fewer satellite operators and an increasingly larger drive toward more autonomy in the satellite diagnostics and control systems. Current methods for detecting and correcting anomalies onboard the satellite and specifically on the ground are primarily ad hoc and manual and, therefore, slow and error-prone. Traditionally, health monitoring and trend analysis of satellite telemetry data have been a time consuming, repetitive, and labour-intensive activity. Operators normally inspect telemetry plots downloaded to the ground stations to determine the current satellite state and health. Given this fact, relieving operators of portions of the telemetry monitoring and anomaly diagnosis task is highly desirable and necessary. It should be recognized that satellite monitoring and fault diagnosis could be automated using advanced decision support systems such as rule-based, expert systems, and intelligent-based methodologies .Conventionally various forms of statistical evaluation techniques are employed and comparisons with prediction and estimation models are performed. However, the evaluations still require extensive human expertise that is subject to error, and could result in catastrophic failures if operators fail to detect and identify critical faults in safety critical components and subsystems such as the ACS. In this work, an advanced decision support system is proposed to accurately and expeditiously monitor the telemetry data in the reaction wheels of a satellite. Our goal is to improve the efficiency, accuracy, and reliability of trend analysis and diagnosis techniques through utilization of estimation and model-based methodologies. Health monitoring of the attitude control system is the process that involves:

i. examining satellite telemetry data,
ii. developing mathematical or functional representations of the data,
iii. analyzing the derived information to formulate an evaluation of the state and condition of the satellite components, and
iv. determining if safety critical trends exist that could lead to catastrophes and loss of the vehicle.

If serious and critical trends are detected, corrective or preventive measures are then identified and reconfiguration and recovery mechanisms are invoked. Specifically, based on the set of fault characteristics and scenarios considered, models that represent the most likely possible system behaviour patterns and structures will be first constructed. Bank of filters based on these models are then designed to operate in parallel at all times [Haykin, 2001; Zang & Xiao, 1998; Zang & Xiao, 1997]. Each filter is designed and tuned to a

particular model (normal or faulty mode) for obtaining a model-based state estimator. The overall state estimate is a "certain" combination of these model-based estimates and the jump or switching in the system mode is modeled as a transition between the estimated models, assuming that this transition is described by a first order Markov chain. By considering various scenarios corresponding to the evolution of the ACS, and based on our preliminary results in [Tudoroiu & Khorasani, 2007; Tudoroiu et al., 2006; Tudoroiu & Zaheeruddin, 2006], we will develop a fault detection, diagnosis, and isolation (FDDI) strategy for the reaction wheel actuators. Subsequently, appropriate remedial actions could be undertaken in the shortest time and as expeditiously as possible to maintain the desired specifications and requirements of the mission. Conventionally, for regulating variables such as temperature, currents, and torques in the ACS various SISO (single input single output) or MIMO (multi input multi output) PI/PID (proportional, integral and derivative), self-tuning, or adaptive feedback control strategies are utilized. The design of a closed-loop control system for achieving the stringent performance specifications of the ACS is a very challenging task since the system:

i. exhibits inherently a highly nonlinear behaviour,
ii. has a multivariable structure, and
iii. is subjected to multiple sources of uncertainties and disturbances.

In this work, we treat the satellite as a MIMO system that is managed by PID controllers yielding good tracking and dynamic performance for the healthy ACS. We then investigate the development of our proposed FDDI strategy for the reaction wheels failures by utilizing bank of interacting Kalman Filter estimators. The FDDI scheme is applied to a highly nonlinear model of the reaction wheel considered as well as a nonlinear attitude dynamics of the satellite [Bialke, 1998]. Regarding the HVAC systems for most of them several failures caused by malfunctions in components, actuators, and sensors can be as result of unexpected interference, or gradual aging of system components. Consequently these failures have a great impact on the energy consumption, thermal comfort and generate severe equipment operating problems. To increase the energy efficiency and equipment reliability, there is a need to develop robust fault detection and diagnosis tools capable of detecting and isolating any sensor, actuator or system component faults so that remedial actions could be taken as soon as possible. The FDDI based on the IMM algorithm is implemented in a simulation environment, and the fault diagnosis results are presented for a several fault scenarios in terms of mode probabilities and mode probability indices.

2. The satellite's ACS model and the discharge air temperature (DAT) system

2.1 The satellite's ACS model

A hypothetical satellite is considered here having a scientific mission to study the Earth. This is a three-axis stabilized satellite which consumes a maximum of approximately 200 Watts of power that is generated by solar arrays and stored power from batteries, of approximately 24 V each, designated by V_{bus}. The attitude control system (ACS) consists of three-axis stabilized system making use of 4-reaction wheels assembly (3 Active + 1 Redundant) type ITHACO. The ACS could be conceptualized as either a MIMO system or as a SISO system if each axis is considered independent and having no interactions with other axes. In this paper, a high fidelity nonlinear representation of a reaction wheel, as shown in Figure 1, is considered. A detailed mathematical model of this reaction wheel is described and derived below. The satellite's attitude control is achieved by using three reaction wheels

to generate control torques in each of the three axes independently. The reaction wheel actuators utilized are essentially torque motors with high inertial rotors. They can spin in either direction and provide one axis of control for each wheel. Each reaction wheel (Roll, Pitch or Yaw) is aligned with one of the body axes of the satellite. The Roll, Pitch or Yaw reaction wheels act as actuators for the Roll, Pitch or Yaw control loops, respectively. Each reaction wheel consists of several internal and external loops that have to be integrated to yield an accurate overall mathematical model. The following loops play an important role in the dynamics of each reaction wheel (refer to Figure 1 and [Bialke, 1998] for further details):

i. The negative feedback EMF torque limiting loop τ_{EMF} due to low bus voltage, V_{bus}, condition that may limit the motor torque at high speeds because of increasing back-EMF voltage gain, K_e, of the motor,
ii. The negative feedback viscous and coulomb friction loop. Viscous friction is generated due to the bearing lubricant, and it has a strong sensitivity to temperature, T. The relationship between temperature and drag torque model is given by:

$$\tau_v = (0.049 - 0.0002(T + 30)) \tag{1}$$

Coulomb friction is caused by friction within bearings, and is independent of the wheel speed and temperature, and therefore is primarily of interest as a disturbance source. This loop is included only for modeling purpose; we don't measure these frictions to be used in the control loop, only we take into consideration their effect in the reaction wheel system.

iii. The negative feedback speed limiter loop is to prevent the flywheel from reaching unsafe speeds,
iv. The motor torque control is included since the motor driver is essentially a voltage controlled current source with a gain G_d. In our research, we consider the motor current I_m to be directly proportional to the torque command voltage. The motor has a torque constant gain K_i, which delivers a torque proportional to the current driver. By changing the torque constant gain K_i, we have the possibility of generating another source of a fault, due to unexpected changes in motor current value, and
v. The torque noise disturbance τ_{noise} is a very low frequency torque variation from bearings due to lubricant dynamics. This torque can be specified as a deviation from the ideal location of rotor at any constant speed, and is connected directly to satellite jitter by the ratio of flywheel inertia to the satellite inertia, according to

$$\theta_{sat} = \theta_{noise} \frac{J}{I_{sat}} \tag{2}$$

The torque noise is assumed as a sine wave having a high pass filter frequency ω_n

$$\tau_{noise} = J\theta_{noise}\omega_n^{\,2} \sin(\omega_n t) \tag{3}$$

where θ_{sat} represents the satellite angular jitter and θ_{noise} represents the torque noise angle. The speed limiter and EMF torque limiting loops use three conditional Heveaside functions to enable the high-gain negative feedback K_s, when the reaction wheel exceeds an established speed threshold ω_s, and to eliminate the voltage drop when the power is not

being drawn from the bus during a deceleration (since the energy is being removed from the wheel). The EMF torque limiting loop could be controlled by the voltage feedback gain, K_f.. The above models and existing governing relationships as shown in Figure 1 could be combined to yield a state-space representation for the reaction wheel, such in [Tudoroiu et al., 2006; Tudoroiu & Khorasani, 2007].

2.2 Discharge Air Temperature (DAT) system

Figure 2 shows a schematic diagram of a DAT loop of a HVAC system. A central air supply provides air at a controlled temperature and water flow rate for use in heating coil, T_{a0} and $\dot{m}_w$ respectively. A heating coil interposed in the central air supply space heats the discharged air using hot water. The temperature of the air leaving the heating coil T_a is controlled by regulating the rate at which the hot water flows through the heating coil as shown by the feedback control loop. The discharged air flow rate is regulated to maintain a predetermined static air pressure within the temperature controlled space. In Figure 2, u represents the hot water flow rate, i.e., the DAT loop subsystem input, and T_a, is the DAT output. The entering air temperature T_{a0} is considered as a disturbance on the system.
The DAT system is modeled as a SISO system as shown by the block diagram in Figure 3.
The model is nonlinear and described by the following equations [Zaheeruddin & Patel, 1995]:

$$\frac{dT_a}{dt} = c_1 h_a \eta_{ov} (\bar{T}_a - \bar{T}_t) + c_2 \dot{m}_a (T_a - T_{a,in}) \tag{4}$$

$$\frac{dT_w}{dt} = c_3 h_w (\bar{T}_t - \bar{T}_w) + c_4 \dot{m}_w (T_w - T_{w,in}) \tag{5}$$

$$\begin{aligned} \frac{d\bar{T}_t}{dt} = \frac{1-\eta_s}{\eta_s + c_5} [c_6 \dot{m}_a (T_a - T_{a,in}) + \frac{c_7}{1-\eta_s} h_w (\bar{T}_t - \bar{T}_w) + \\ + (c_8 + \frac{c_9}{1-\eta_s}) h_a \eta_{ov} (\bar{T}_a - \bar{T}_t)] \end{aligned} \tag{6}$$

For the simulations we use the following values for the coefficients:

$$c_1 = -1.2046, c_2 = -38.9034, c_3 = 4.5714 \times 10^{-5}, c_4 = -0.2023,$$

$$c_5 = 1.1192, c_6 = 38.9034, c_7 = -1.4926 \times 10^{-5}, c_8 = 1.2046,$$

$c_9 = 4.8995 \times 10^{-4}$, and the air and water heat transfer coefficients $h_a, h_w,$ the sensitive efficiency quadratic functions η_s, η_{ov} are given by:

$$h_a = -17.58 \dot{m}_a{}^2 + 70.562 \dot{m}_a + 8.1796 , \tag{7}$$

$$h_w = 1403.2 (\dot{m}_w)^{0.8} , \tag{8}$$

$$\eta_s = 0.16375 \dot{m}_a^2 - 0.39483 \dot{m}_a + 0.92805 , \tag{9}$$

$$\eta_{ov} = 1 - 0.9(1 - \eta_s)\,. \tag{10}$$

The variation ranges for the disturbance inputs $\dot{m}_a, T_{a,in}, T_{w,in}$, and the control input $\dot{m}_w$, are given by:

$$\dot{m}_a \in [0.1,\ 0.8]\left[\frac{kg}{s}\right], T_{a,in} \in [16, 22][^0C],\ T_{w,in} \in [35, 50][^0C]$$

The variables that appear in this DAT model have the following significance:

$T_a\ [^0C]$ -the air temperature leaving the heating coil,

$T_w\ [^0C]$ - the hot water supply temperature, with their average values given by

$$\overline{T}_a = \frac{T_a + T_{a,in}}{2}, \overline{T}_w = \frac{T_w + T_{w,in}}{2},$$

$\overline{T}_t\ [^0C]$ - the average tube temperature, $T_{a,in}\ [^0C]$ -the inlet air temperature leaving the heating coil, $T_{w,in}\ [^0C]$ -the inlet water supply temperature, $\dot{m}_a \left[\frac{kg}{s}\right]$-the input air flow rate, and $\dot{m}_w \left[\frac{kg}{s}\right]$-the water flow rate.

The input of the simplified *SISO* model is hot water flow rate, $\dot{m}_w$, $u(k)$, and the output is the temperature of air leaving the heating coil, T_a [ºC], $y(k)$. Hot water supply temperature T_w[ºC] and the average tube temperature $\overline{T}_t$ [ºC] act as disturbances on the DAT loop of HVAC system. Also such as input disturbances could be considered $\dot{m}_a, T_{a,in}$, and $T_{w,in}$. In practice the hot water flow rate is regulated such that the temperature of air leaving the heating coil is maintained closed to a chosen set-point. In this representation the heating coil output temperature set point is more directly related to the overall DAT subsystem performance, and the model uncertainties are due to variable heat and mass transfer rates.

The equivalent discrete time space system representation of the DAT system (4)-(6) has the following form:

$$\begin{aligned} x_1(k+1) = x_1(k) + c_1 h_a(k)\eta_{ov}(k)T_s(\overline{x}_1(k) - x_3(k)) + \\ c_2 T_s(x_1(k) - p_1(k))p_2(k) \end{aligned} \tag{11}$$

$$\begin{aligned} x_2(k+1) = x_2(k) + c_3 h_w(k)T_s(x_3(k) - \overline{x}_2(k)) + \\ c_4 T_s(x_2(k) - p_3(k))u(k) \end{aligned} \tag{12}$$

$$\begin{aligned} x_3(k+1) = x_3(k) + \frac{1-\eta_s}{\eta_s + c_5} T_s[c_6 u(x_1(k) - p_2(k))p_1(k) + \\ \frac{c_7}{1-\eta_s} h_w(k)(x_3(k) - \overline{x}_2(k))p_2(k) + \\ (c_8 + \frac{c_9}{1-\eta_s}) h_a(k)\eta_{ov}(k)(\overline{x}_1(k) - x_3(k))] \end{aligned} \tag{13}$$

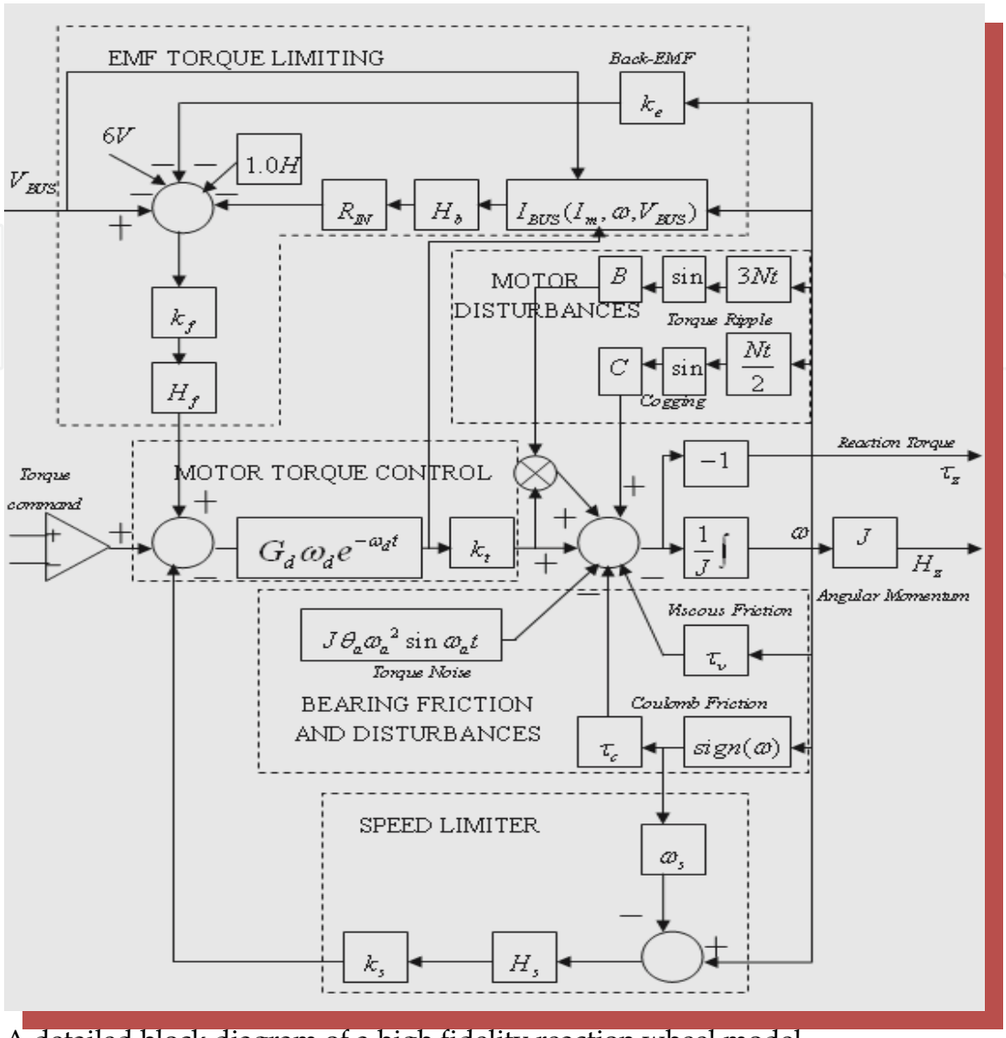

Fig. 1. A detailed block diagram of a high fidelity reaction wheel model.

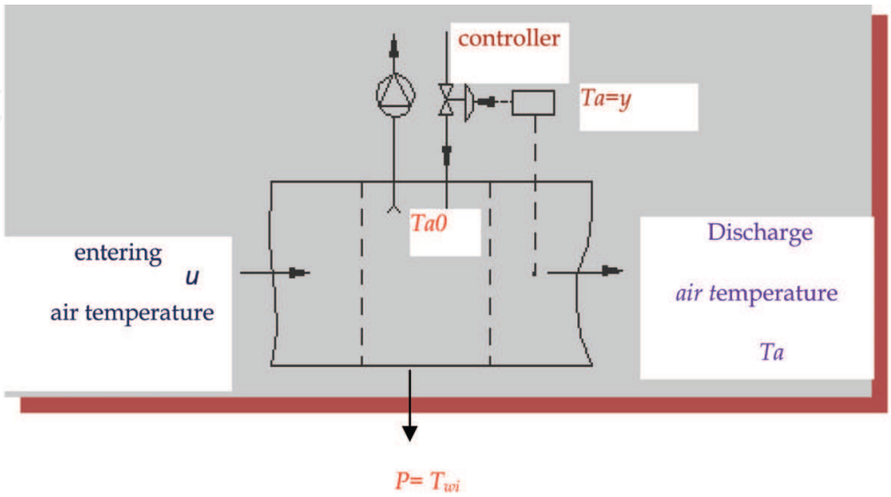

Fig. 2. Schematic diagram of DAT system

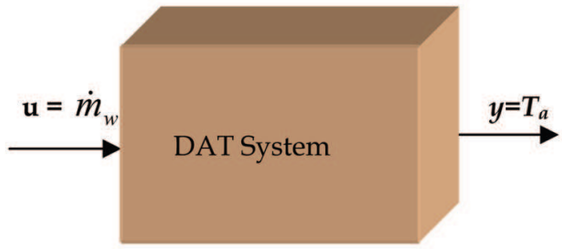

Fig. 3. SISO DAT oriented system

$$y(k) = x_1(k) \tag{14}$$

where

$x(k) = [x_1(k) \;\; x_2(k) \;\; x_3(k)]^T = [T_a(k) \;\; T_w(k) \;\; \overline{T}_t(k)]^T$ represents the state space vector,

$u(k) = \dot{m}_w(k)$ is the DAT subsystem input,

$y(k) = [T_a(k)]$ is the DAT subsystem output, and

$p(k) = [p_1(k) \;\; p_2(k) \;\; p_3(k)]^T = [T_{a,in}(k) \;\; \dot{m}_a(k) \;\; T_{w,in}(k)\;]^T$ represents the disturbance input vector. In simulation environment we consider the sampling time T_s = 4 seconds.

The sensitive efficiency quadratic functions η_s, η_{ov} and the time variable water heat transfer coefficients h_a, h_w, become:

$$\eta_s(k) = 0.16375 p_2{}^2(k) - 0.39483 p_2(k) + 0.92805 \tag{15}$$

$$\eta_{ov}(k) = 1 - 0.9(1 - \eta_s(k)) \tag{16}$$

$$h_a(k) = -17.58 p_2{}^2(k) + 70.562 p_2(k) + 8.1796 \tag{17}$$

$$h_w(k) = 1403.2(u(k))^{0.8} \tag{18}$$

The average values of the states $x_1(k)$ and $x_2(k)$ are given by

$$\overline{x}_1(k) = \frac{x_1(k) + x_{1,in}(k)}{2}, \overline{x}_2(k) = \frac{x_2(k) + x_{2,in}(k)}{2} \tag{19}$$

where

$$x_{1,in}(k) = T_{a,in}(k),$$

$$x_{2,in}(k) = T_{w,in}(k)\,.$$

The dynamics of the valve actuator is integrated in the plant dynamics, and will be represented by a nonlinear block with backlash characteristic of dead zone width =2r, such in Figure 4.

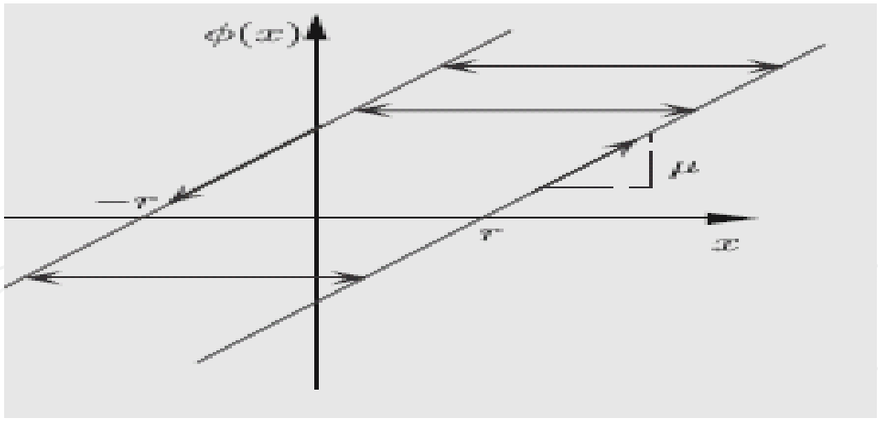

Fig. 4. The backslash nonlinearity

The input-output behaviour of the backlash nonlinearity can be described by two modes of operation, as either tracking or in the dead zone:
Tracking described by the following differential equation:

$$\dot{w} = \mu \dot{y} \tag{20}$$

with the solution given by:

$$w = \mu(y - r) \quad \text{for } \frac{dy}{dx} > 0, \text{ and} \tag{21}$$

$$w = \mu(y + r) \quad \text{for } \frac{dy}{dx} < 0 \tag{22}$$

Dead zone described by the following differential equation:

$$\dot{w} = 0 \quad | w - \mu y | \leq \mu r \tag{23}$$

where r is the dead zone width and μ is the slope of tracking region such as depicted in the Figure 4, with

$$y = \phi(x) \text{ , and} \tag{24}$$

$$w(t) = \phi(\phi_0, x([0,t)) = \Phi[x, \phi_0](t) \text{ , } t \in [0,T] \tag{25}$$

Unlike memory less nonlinearities, hysteresis output at any given time is function of the entire history of the input, and the initial condition of the output, ϕ_0 .

3. Kalman filter estimation techniques

3.1 Extended Kalman Filter (EKF)

Consider the dynamics of a *linear* stochastic system expressed in the state-space difference representation

$$x_{k+1} = Fx_k + Gu_k + w_k \tag{26}$$

$$y_k = Hx_k + v_k \tag{27}$$

where w_k and v_k are the process and measurement noise, respectively, that are assumed to be independent white Gaussian random processes with zero mean and

$$E[w_n w_k^T] = \begin{cases} Q_w, n = k \\ 0, n \neq k \end{cases}, \quad E[v_n v_k^T] = \begin{cases} R_v, n = k \\ 0, n \neq k \end{cases} \tag{28}$$

The process and measurement noise have normal probability distributions governed by

$$\mathrm{p}(w) \sim N(0, Q_w), \ \mathrm{p}(v) \sim N(0, R_v) \tag{29}$$

The covariance matrices Q_w (process noise covariance) and R_v (measurement noise covariance) might change with each time step or measurement, but in our approach we assume that they are constant. Due to the process noise injected in the state space equation (26)-(27), the state vector $x_k \in R^n$ becomes random variable with its distribution approximated by a Gaussian distribution function $\mathrm{p}(x) \sim G(\hat{x}, P_x)$. The general formulation of EKF algorithm used for the state estimation of the dynamical system (26)-(27) is well presented in the literature and we recommend for documentation some of the several fundamental papers such as [Plett, 2004; Haykin 2003;Joseph, 2003; Wan & Merwe, 2000; Julier & Uhlman, 1997]. The covariance matrices Q_w (process noise covariance) and R_v (measurement noise covariance), together with the initial error covariance $P_{0|0}$ are the three tuning parameters in the EKF algorithm. The matrices Q_w and R_v are determined empirically and account for uncertainty in the tracking data. Setting these matrices "properly" significantly contributes in making the EKF filter robust. The error covariance matrix P indicates uncertainty in the state estimate and provides criterion for the error bound.

3.2 Unscented Transform Techniques (UTT)

Compared to EKF the UKF addresses the approximation issues presented in [Haykin, 2003; Joseph, 2003; Wan & Merwe, 2000; Julier & Uhlman, 1997]. The state distribution is represented by a Gaussian Random Variable, specified using a minimal set of carefully chosen sigma points. These sigma points completely capture the true mean and covariance of the Gaussian random variable, and when propagated through the true non-linear system, capture the posterior mean and covariance accurately until the 3rd order (Taylor series expansion) for any nonlinearity. The Unscented Transformation (UT), is a method for calculating the statistics of a random variable, which undergoes a nonlinear transformation. Consider propagating a random variable x (dimension L) through a nonlinear function, $y = g(x)$. We assume that x has the mean $\bar{x}$ and the covariance P_x. To calculate the statistics of y we will build a matrix X of $2L+1$ sigma vectors X_i (with corresponding weights W_i), as follows:

$$
\begin{aligned}
&X_0 = \overline{x} \\
&X_i = \overline{x} + (\sqrt{(L+\lambda)\times P_x})_i, i = 1,2...,L \\
&X_i = \overline{x} - (\sqrt{(L+\lambda)\times P_x})_{i-L}, i = L+1,...,2L \\
&W_0^m = \frac{\lambda}{L+\lambda} \\
&W_0^c = \frac{\lambda}{L+\lambda} + (1-\alpha^2+\beta) \\
&W_i^m = W_i^c = \frac{1}{2\times(L+\lambda)}, i = 1,2...,2L
\end{aligned}
\tag{30}
$$

where the parameter λ is selected in deterministic manner

$$\lambda = \alpha^2 \times (L+\kappa) - L \tag{31}$$

and α represents a scaling parameter, which determines the spread of the sigma points around mean state value $\overline{x}$ and is usually set to a small positive value. k is a secondary scaling parameter which is usually set to 0, β is used to incorporate prior knowledge of the distribution of x (for Gaussian distribution, β =2 is optimal), and $\sqrt{(L+\lambda)P_x})_i$ is the *i-th* row of the matrix square root. The Unscented Transform determine the mean and covariance of system output y by approximation, using a weighted sample mean and covariance of the posterior sigma points. A simple example is shown in Figure 5 for a two-dimensional system. The left plot shows the true mean and covariance propagation using Monte-Carlo sampling [Haykin, 2003; Joseph, 2003; Julier & Uhlman, 1997], the center plots show the results using a linearization approach as would be done in the Unscented Transform (UT), and the right plots show the performance of the UT.

$$
\begin{aligned}
&Y_i = g(X_i) \\
&\overline{y} \approx \sum_{i=0}^{2L} W_i^m Y_i \\
&P_y \approx \sum_{i=0}^{2L} W_i^c [Y_i - \overline{y}][Y_i - \overline{y}]^T
\end{aligned}
\tag{32}
$$

3.3 Unscented Kalman Filter (UKF) technique

The Unscented Kalman Filter (UKF) technique is based on the unscented transformation (UT) [Haykin, 2003; Joseph, 2003; Wan & Merwe, 2000; Julier & Uhlman, 1997] and addresses the general problem of state estimation $\mathbf{x}_k \in R^n$ of a discrete-time controlled process that is governed by the nonlinear stochastic difference state-space equation with a measurement $\mathbf{y}_k \in \mathbf{R}^m$ that is given by the output equation

$$\mathbf{x}_{k+1} = f(\mathbf{x}_k, \mathbf{u}_k) + \mathbf{w}_k \tag{33}$$

$$\mathbf{y}_k = g(\mathbf{x}_k, \mathbf{u}_k) + \mathbf{v}_k \tag{34}$$

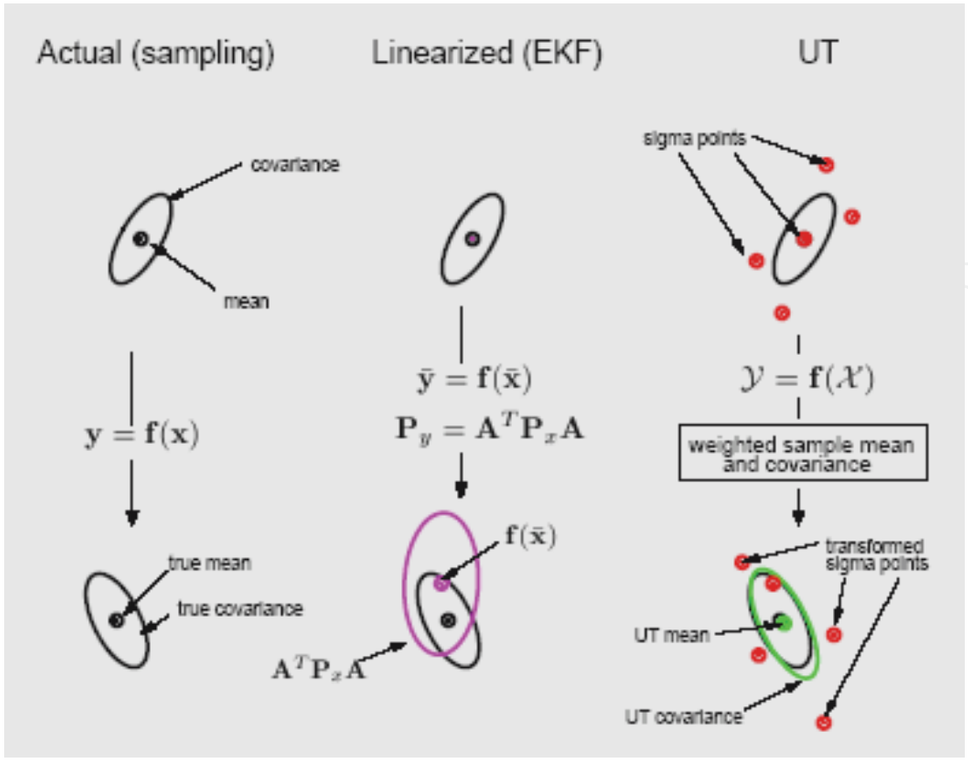

Fig. 5. Two-dimensional example of the Unscented Transform [1]-[4]

The random variables $\mathbf{w}_k$ and $\mathbf{v}_k$ representing the process and measurement noise injected to drive the system dynamics are generated by the additive noise sources. They are assumed to be independent, zero mean, white, and with normal probability distributions:

$$p(\mathbf{w}) \sim N(0, \mathbf{Q}_\mathbf{w})$$

$$p(\mathbf{v}) \sim N(0, \mathbf{R}_\mathbf{v}) \tag{35}$$

The covariance matrices $\mathbf{Q}_w$ (process noise covariance) and $\mathbf{R}_v$ (measurement noise covariance) might change with each time step or measurement, but in our approach we assume they are constant. Due to the process noise injected in the state space equation the state vector $\mathbf{x}_k \in \mathbf{R}^n$ becomes random variable with its distribution approximated by a Gaussian distribution function:

$$p(\mathbf{x}) \sim G(\hat{\mathbf{x}}, \mathbf{P}_\mathbf{x}) \tag{36}$$

The vital operation performed in the Kalman Filter is the propagation of a Gaussian random state variable $\mathbf{x}_k \in \mathbf{R}^n$ through the system dynamics. In the Extended Kalman Filter (EKF) estimator the Gaussian random state variable $\mathbf{x}_k \in \mathbf{R}^n$ is propagated analytically through the first-order linearization of the nonlinear system.
This can introduce large errors in the true posterior mean and covariance of the transformed Gaussian random state variable, which may lead to sub-optimal performance and sometimes divergence of the filter. The UKF estimator approach is developed such as an

alternative to the EKF estimator and addresses this problem by using a deterministic sampling approach.

Using the principle that a minimal set of carefully chosen sample points can be used to parameterize mean and covariance, the UKF estimator yields superior performance compare to EKF estimator, specially for nonlinear systems. These sample points completely capture the true mean and covariance of the Gaussian random state variable $\mathbf{x}_k \in \mathbf{R}^n$, and are propagated through the true nonlinear system dynamics. The main advantage of the UKF estimator is that does not require the calculation of the Jacobean matrices that could lead to implementation difficulties In this work we developed an augmented UKF architecture [Haykin, 2003; Joseph, 2003; Wan & Merwe, 2000; Julier & Uhlman, 1997].

The algorithm is developed to compute a collection of sigma points corresponding to the state vector $\mathbf{x}_k$ or noise signals $\mathbf{w}_k$ and $\mathbf{v}_k$ stored in the column of the $L \times (2L+1)$ sigma point matrix $\mathbf{X}_{k-1}$, where $L = \dim(X) + \dim(W) + \dim(V)$.

4. Design of the IMM Fault Detection and Diagnosis (FDDI) strategy

4.1 Jump Markov linear hybrid dynamic model

The multiple model approach for fault detection and diagnosis (FDD) assumes that the actual system at any time can be modeled sufficiently accurately by the following jump Markov hybrid nonlinear system:

$$x(k+1) = F(k, m(k+1), x(k), u(k)) + T(k, m(k+1))w(k, m(k+1)),\ x(0) \sim N(\hat{x}_0, P_0) \quad (37)$$

$$z(k) = G(k, m(k), x(k), u(k)) + v(k, m(k)) \quad (38)$$

The mode of the system (normal or faulty) at time k is selected by a discrete process m_j and modeled as a s-state, first-order Markov chain with transition probabilities $\pi_{ij}(k)$ given by:

$$\pi_{ij}(k) = P\{m_j(k+1) \mid m_i(k)\},\ \forall m_i, m_j \in S \quad (39)$$

and

$$0 \le \pi_{ij}(k) \le 1,\ i = \overline{1,N},\ j = \overline{1,N},\qquad \sum_j \pi_{ij}(k) = 1,\ \ i = \overline{1,N} \quad (40)$$

The initial state distribution of the Markov chain is $\pi(0) = [\pi_1\ \pi_2\ \pi_3\ .....\pi_N]$, where

$$0 \le \pi_j \le 1,\ \forall j = \overline{1,N},\ \sum_{j=1}^{N} \pi_j = 1 \quad (41)$$

and where $x(k)$ is the state vector, $z(k)$ is the mode-dependent measurement vector, and $u(k)$ is the control input vector. The process and measurement noise vectors $w(k)$ and $v(k)$, respectively, are mutually independent, additive, white Gaussian of zero mean and covariance matrices $Q_w(k)$ and $R_v(k)$, and are independent of the initial state $x(0)$. In expression (39), P{.} denotes the probability operator. The event that m_j is in effect at time

k is denoted as $m_j(k) = \{m(k) = m_j\}$, and $S = \{m_1, m_2, ..., m_N\}$ represents the set of all possible system modes. The system (37)-(38) may jump from one such system to another at a random time. It can be observed from (37) that the state vector observations are in general noisy and dependent. Therefore, the mode information is embedded in the measurement sequence. The system mode sequence is an indirectly observed Markov chain, from which the transition probability matrix $\pi = \{\pi_{ij}\}$ represents a design parameter. The FDD problem for the above hybrid system (37)-(38) can be stated as that of determining the current model state. In other words, it involves determining whether the normal or a faulty mode is currently in effect from a sequence of noisy observations. How to design set of modes to represent the possible system modes is a key issue in multiple model approach, which is problem-dependent. This design should be achieved by attempting to have models (approximately) that represent or cover all possible system modes at any given time. This represents the model set design that is critical for multiple model based FDD. To design a good set of models requires *a priori* knowledge of possible faults in the system. These issues are formally described in the next subsection.

4.2 IMM Fault Detection and Diagnosis and Isolation (FDDI) strategy

In application of multiple model estimation techniques for fault detection and diagnosis, the following tasks should be implemented:

i. model set design,
ii. filter selection,
iii. estimate fusion, and
iv. filter re-initialization.

Filter selection deals with the problem of selecting a model-based recursive filter such as an unscented Kalman Filter (UKF) for each model of the nonlinear system. The estimate fusion task combines model-conditional estimates to obtain an overall estimate. Towards this end, three approaches could be investigated, namely soft, hard and random decisions. The procedure for reinitializing each single-model based filter from time to time is of significant importance for multi-model estimation. The simplest approach for reinitializing each filter is to use its previous state estimate and filter covariance at the current cycle. In this case filters are operating in parallel and no interactions exist among them. However, this may lead to unsatisfactory performance when the system structure or its mode changes. For this reason, it would be more appropriate to reinitialize each filter using the previous overall state estimate and covariance matrix which does lead to an interacting multiple model estimation technique. For each faulty mode corresponding to a set of possible ACS reaction wheel or HVAC faults and a normal operating mode, one can apply an EKF or UKF based on measurements collected from the reaction wheel or valve actuators**.** The input considered can be taken as the torque command voltage vector ***u,*** or water flow rate**.** The dynamics of a Kalman Filter estimation technique associated with each mode is described by the following nonlinear state space representation:

$$\begin{aligned} x_j(k+1) &= F_j(k, x_j(k), u_j(k)) + T_j(k) w_j(k) \\ z_j(k) &= G_j(k, x_j(k), u_j(k)) + v_j(k) \end{aligned} \tag{42}$$

where the subscript j denotes the quantities pertaining to mode m_j. The nonlinear functions F_j, G_j and the weighting matrix T_j may have different structures for different values of j. The process noise and measurement noise vectors w_j and v_j are white Gaussian of zero mean with covariance matrices Q_{wj} and R_{vj}, respectively. In principle the probability of a given model matches the system mode provides the required information for the fault detection and diagnosis. Taking into account historical behaviour of modes at time k ensures that the interacting multiple model (IMM) algorithm yields a good estimate. Consequently, exponential increase in complexity of a detection algorithm is avoided by mixing previous estimates at beginning of each cycle. The model probabilities provide an indication of the mode in effect at any given time, and therefore can provide an indication of the reaction wheel actuator fault. By using model probabilities information, both fault detection and diagnosis can be achieved. This decision making process is formally stated according to:

$$\begin{aligned} &\mu_j(k+1) = \max_j \mu_j(k+1) = \mu \\ &If \quad \mu > \mu_T \quad then \quad \text{mode} \quad j \quad is \quad faulty \\ &Otherwise \quad no \quad fault \quad occurs \end{aligned} \tag{43}$$

where $\mu_{Threshold}$ represents the fault detection threshold value. The interacting estimation algorithm runs each parallel filter banks only once in each cycle. Each of these filters at time $t_{k+1} = k+1$ has its own input, the state estimate at time t_k, $\hat{x}^0(k|k)$, and its own covariance matrix, $P^0(k|k)$, which form a valid quasi-sufficient statistics of all the past information, under the assumption that model of each filter matches the system mode. The above decision rule yields not only fault detection capability but also information about the type (sensor or actuator), the location (which sensor or actuator), the size (total failure or partial failure with fault severity), and the fault occurrence time.

4.3 Interacting Multiple Model (IMM) algorithm

A detailed procedure for an IMM algorithm that utilizes the standard Kalman Filter estimation technique is included in references [Zhang & Xiao, 1997; Narendra & Balakrishnan, 1997; Zhang & Xiao, 1998]. Similarly, the steps for an IMM algorithm that utilizes an UKF estimation technique are also developed in [Tudoroiu & al., 2006, Tudoroiu & Zaheeruddin, 2006, Tudoroiu & Khorasani, 2005]. Based on the standard IMM algorithm described in details in [Zhang & Xiao, 1997; Zhang & Xiao, 1998] we could embed without difficulties the dynamics of the EKF or UKF estimation techniques to obtain an IMM_EKF or IMM_UKF structures. A simplified flowchart representing the FDDI scheme with the process dynamics of the IMM_ EKF and IMM_UKF estimators is shown in Figure 6. The results of applying EKF and UKF algorithms for fault detection and diagnosis (FDDI) of the faults in reaction wheel actuators (ACS) of the satellite and in valve actuators (HVAC systems). These results will be presented in the next section.

Parameter Settings

The set of parameters chosen for the EKF and UKF algorithms is given by

$$\alpha = 0.0001,\ k = 0,\ \beta = 2,\ \mathbf{P}_0 = 1*10^{-6}*\mathbf{I_3},\ \mathbf{Q}_w = 2*10^{-6}*\mathbf{I_3},\ R_v = 10^{-6}.$$

5. Simulation results

5.1 ACS systems

EKF and UKF-based interacting multiple model (IMM) algorithms are now applied for fault detection and diagnosis of a reaction wheel under different kinds of uncertainty (unknown model structure and parameters). In this work, we consider only transitions between the normal mode and faulty modes as well as between faulty modes and the normal mode. The root-causes of faults injected to the reaction wheels are due to the following sources:

i. unexpected viscous friction changes generating anomalies in the temperature T,
ii. unexpected changes in the bus voltage V_{bus}, and
iii. loss of effectiveness in the motor torque as represented by unexpected changes in the coefficient k_t.

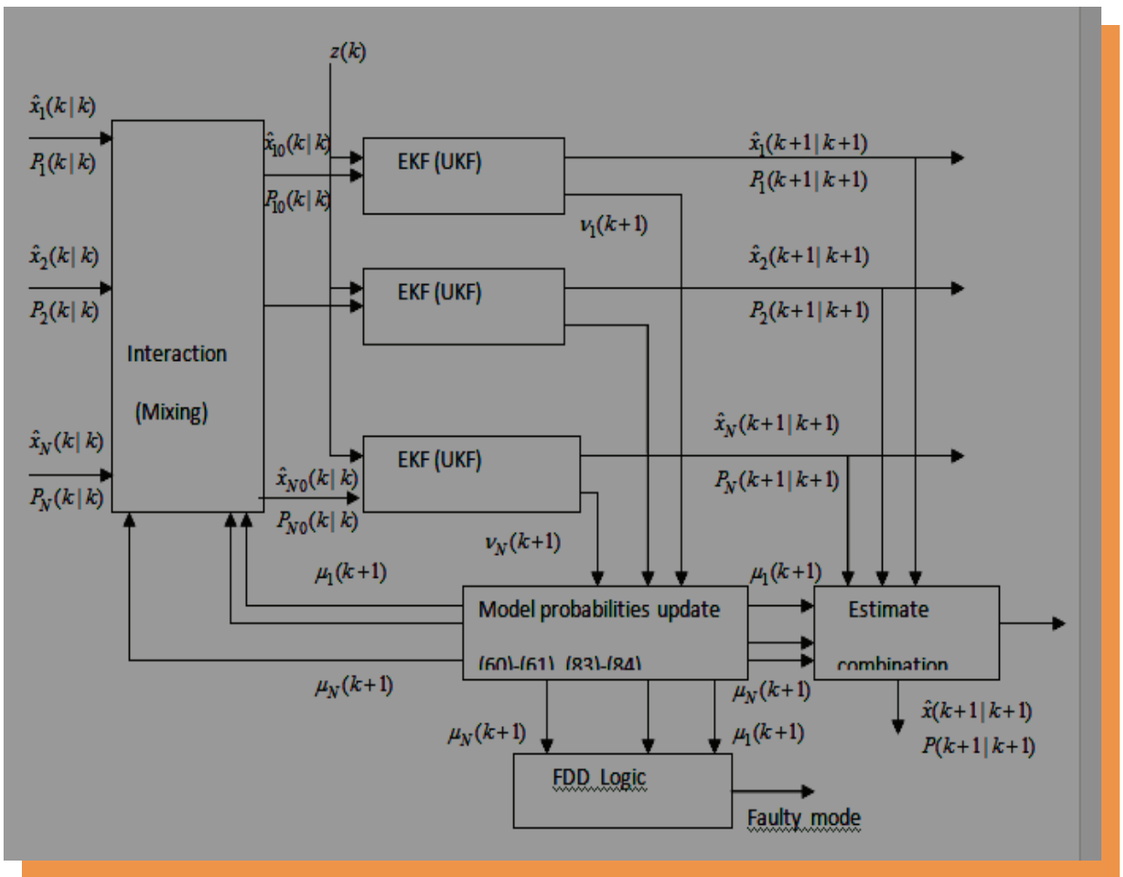

Fig. 6. FDD Block Scheme

Let us now to designate by $(z_1,u_1),(z_2,u_2),(z_3,u_3),(z_4,u_4)$ measurement observations and inputs of the filter banks for the normal mode, first, second, and third faulty modes, respectively. We also designate by $(z_{23},u_{23}),(z_{24},u_{24}),(z_{34},u_{34})$ measurement observations and inputs of the filter banks for simultaneous two faulty modes $(z_2z_3,u_{23}),(z_2z_4,u_{24}),(z_3z_4,u_{34})$, respectively. These modes are labelled from j=1 to j=7 as an alternative to a mode probability graphical representation. In this way it is easier to

identify the occurrence and dynamic evolution of fault modes within each window horizon. These modes have the following specifications:

i. The normal mode (z_1,u_1), labelled j=1, is generated according to the nonlinear state equations corresponding to the nominal parameters, $T_1 = 30\,[^0C]$, $k_{t_1} = 0.029$, and $V_{bus_1} = 24[V]$.

ii. The faulty mode (z_2, u_2), labelled j=2, is generated by an abnormal increase of temperature from $T_1 = 30[^0C]$ to $T_2 = 200[^0C]$, $k_{t_2} = 0.029$, and $V_{bus_2} = 24[V]$.

iii. The faulty mode (z_3, u_3), labelled j=3, is generated by a sudden change of V_{bus} from $V_{bus_1} = 24[V]$ to $V_{bus_3} = 12[V]$, $T_3 = 30\,[^0C]$, and $k_{t_3} = 0.029$.

iv. The faulty mode (z_4, u_4), labelled j=4, is generated by a sudden change in the motor current corresponding to a loss of effectiveness of k_t from $k_{t_1} = 0.029$ to $k_{t_4} = 0.002$, $T_4 = 30\,[^0C]$, and $V_{bus_4} = 24[V]$.

v. The faulty mode (z_{23}, u_{23}), labelled j=5, is generated by an abnormal increase of temperature from $T_1 = 30[^0C]$ to $T_5 = 100[^0C]$ and a sudden change of V_{bus} from $V_{bus_1} = 24[V]$ to $V_{bus_5} = 12[V]$, and $k_{t_5} = 0.029$.

vi. The faulty mode (z_{24}, u_{24}), labelled j=6, is generated by an abnormal increase of temperature T from $T_1 = 30^0[C]$ to $T_6 = 100[^0C]$ and a sudden change in the motor current corresponding to a loss of effectiveness k_t from $k_{t_1} = 0.029$ to $k_{t_6} = 0.002$, and $V_{bus_6} = 24[V]$.

vii. The faulty mode (z_{34}, u_{34}), labelled j=7, is generated by a sudden change of V_{bus} from $V_{bus_1} = 24[V]$ to $V_{bus_7} = 12[V]$ and a change in the motor current corresponding to a loss of effectiveness of k_t from $k_{t_1} = 0.029$ to $k_{t_7} = 0.002$, and $T_7 = 30^0[C]$.

The specific level of process and measurement noise, and the selected parameters and initialization settings are given below:

$$\hat{x}_1 = \hat{x}_2 = \hat{x}_3 = \hat{x}_4 = \begin{bmatrix} 0 \\ 0 \end{bmatrix},\ P_1 = P_2 = P_3 = P_4 = 10^{-4}\begin{bmatrix} 1 & 0 \\ 0 & 1 \end{bmatrix},$$

$T_1 = T_2 = T_3, = T_4 = \begin{bmatrix} 1 & 0 \\ 0 & 1 \end{bmatrix}$, the process and measurement noise covariance matrices are

$$Q_1 = Q_2 = Q_3 = Q_4 = 2\times 10^{-2}\begin{bmatrix} 1 & 0 \\ 0 & 1 \end{bmatrix},\ R_1 = R_2 = R_3 = R_4 = 5\times 10^{2}\begin{bmatrix} 1 & 0 \\ 0 & 1 \end{bmatrix},$$

$\mu_1(1,1) = \mu_2(1,1) = \mu_3(1,1) = \mu_4(1,1) = \frac{1}{N}$, N = 4 represents the number of modes, the

threshold mode probability is $\mu_{Threshold} = 0.3$, and the IMM transition mode probability is selected as $\pi = \begin{bmatrix} \frac{117}{120} & \frac{1}{120} & \frac{1}{120} & \frac{1}{120} \\ \frac{3}{120} & \frac{117}{120} & 0 & 0 \\ \frac{3}{120} & 0 & \frac{117}{120} & 0 \\ \frac{3}{120} & 0 & 0 & \frac{117}{120} \end{bmatrix}$.

The simulation results are presented in Figure 7.

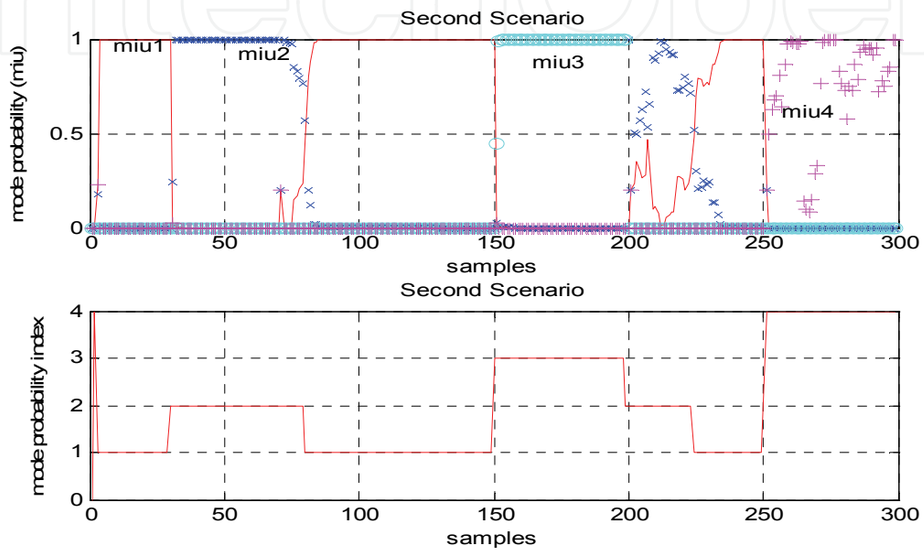

(a)

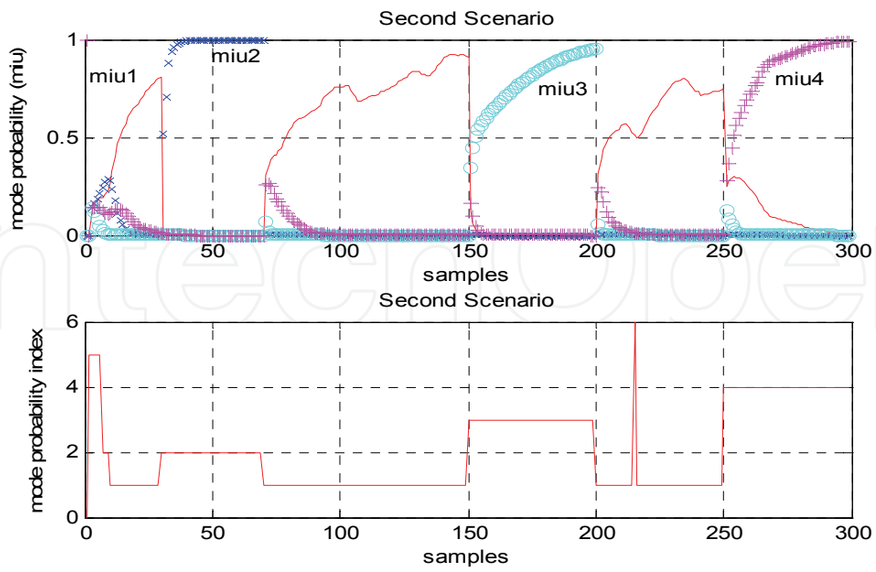

(b)

Fig. 7. The evolution of the mode probability and of the index of the mode probability for the second scenario.

It should be noted that there are short transient responses in the first window horizon [0, 30] and in the sixth window horizon [200, 250] for the IMM UKF algorithm (Figure 7(b)), but a long transient response time of at least 25 samples inside the window horizon [200, 250], for the IMM EKF algorithm (Figure 7(a)). Results reveal that a very good faulty mode detection and classification are obtained with a very fast transient response for the EKF algorithm and a small transient response for the UKF algorithm. For the simulation purpose we consider in our research the sequence of multiple fault modes (second scenario) $z = [z_1\ z_2\ z_1\ z_3\ z_1\ z_4]$, $u = [u_1\ u_2\ u_1\ u_3\ u_1\ u_4]$, where the first, second, and the third wheel's fault occur at the beginning of window horizons [30,70], [150,200], and [250,300], respectively. These faults persist for the duration of 40, 50, and 50 samples, respectively within each window. The evolution of mode probabilities and their index for this scenario are presented in Figures 7(a) and 7(b).

5.2 HVAC systems

The simulation results for the UKF estimator and IMM_UKF analysis approach in the simple estimation and fault detection (valve leakage) cases of the HVAC systems are presented in Figures 8-11. The step responses of the healthy DAT system ($\propto$ = r = 0) and of the faulty modes ($\propto$ = r =2, 4, and 6, representing different severity levels of the valve leakage) are represented and described in detail in [Tudoroiu & Zaheeruddin, 2006, Tudoroiu & Zaheeruddin 2005]. These responses reveal a progressive degradation of the system performance with the increasing of the backlash width $\propto$. In practice, it is very important to detect all these intermediate phases of progressive increase in backlash width to avoid complete failure of the valve actuator and consequently the total degradation of the system performance.

For state estimation purpose we consider the following two cases:

a. State estimation with the same state initial conditions with the process model, as in Figure 8:
   (15[^{o}C], 35[^{o}C] ,34[^{o}C]), p_1=10[^{o}C], p_3=40[^{o}C])
b. State estimation with different state initial conditions than the process model, as in Figure 9:
   (20[^{o}C], 38[^{o}C] ,37[^{o}C]), p_1=10[^{o}C], p_3=40[^{o}C]) for process model and (25[^{o}C], 32[^{o}C], 30[^{o}C]), p_1=10[^{o}C], p_3=40[^{o}C]) the initial conditions for the state estimates.

The simulations results presented in Figures 8-9 reveal the robustness of the UKF algorithm to the changes in the initial conditions of the state estimates. The IMM_UKF algorithm could be applied for a wide engineering applications field for estimation and fault detection, diagnosis and isolation (FDDI) of stochastic systems under different kinds of uncertainties (unknown model structure or parameters) or system failures (valve leakage, stuck-open valve, stuck close valve). In our paper we have applied IMM_UKF algorithm to detect the following faulty modes:

1. **First scenario (healthy system)**, labeled by j=1 is obtained for the following parameters values: p_1=10, p_2=0.8, p_3=40.
2. **Second scenario (first fault)**, labeled by j=2 is obtained for p_1=16, p_2=0.8, p_3=40.
3. **Third scenario (second fault)**, labeled by j=3 is obtained for p_1=10, p_2=0.8, p_3=40.
4. **Fourth scenario (third fault)**, labeled by j=4 is obtained for p_1=10, p_2=0.6, p_3=50.

For the simulation purposes we consider the following scenarios:

i. $z = z_j, u = u_j$, $j = 1,2,3,4.$

ii. $z = [z_1\ z_2\ z_1], u = [u_1\ u_2\ u_1]$, when the first actuator's failure occurs inside the horizon window [50,150].

iii. $z = [z_1\ z_3\ z_1], u = [u_1\ u_3\ u_1]$, when the second actuator's failure occurs inside the horizon window [150, 200].

iv. $z = [z_1\ z_4\ z_1], u = [u_1\ u_4\ u_1]$, when the third actuator's failure occurs inside the horizon window [150, 250].

v. $z = [z_1\ z_2\ z_1\ z_3\ z_1\ z_4\ z_1], u = [u_1\ u_2\ u_1\ u_3\ u_1 u_4\ u_1]$, when the first actuator's failure occurs inside the horizon window [50,100], the second actuator's failure inside the horizon window [150, 200], and the third actuator's failure inside the horizon window [250, 300]. In this paper we consider only the transitions between the normal mode and the fault modes, and also between the fault modes and the normal mode. The output measurements z_1, z_2, z_3, z_4 could be obtained from the deterministic part of the model equations. The process will be initialized by the following values:

$$\hat{x}_1 = \hat{x}_2 = \hat{x}_3 = \hat{x}_4 = \begin{bmatrix} 0 \\ 0 \\ 0 \end{bmatrix}, P_1 = P_2 = P_3 = P_4 = diag(0.0001,\ 0.0001,\ 0.0001)\ ,$$

$$T_1 = T_2 = T_3 = T_4 = \begin{bmatrix} 1 & 0 & 0 \\ 0 & 1 & 0 \\ 0 & 0 & 1 \end{bmatrix},$$

The initial values of the mode probabilities are assumed to be equal: $\mu_1 = \mu_2 = \mu_3 = \mu_4 = \frac{1}{n} = 0.25$, where n = 4, represents the number of modes, the threshold mode probability $\mu_{Threshold} = 0.02$, and the transition mode probability used for simulations is

$$\pi = \begin{bmatrix} \frac{117}{120} & \frac{1}{120} & \frac{1}{120} & \frac{1}{120} \\ \frac{3}{120} & \frac{117}{120} & 0 & 0 \\ \frac{3}{120} & 0 & \frac{117}{120} & 0 \\ \frac{3}{120} & 0 & 0 & \frac{117}{120} \end{bmatrix}$$

It seems that the last scenario is more complex and we will present the simulation results only for this sequence of multiple faults such in Figures 10-11. In Figure 10 is presented the evolution of the mode probabilities and in Figures 11 is presented the probability index of the active fault. These simulation results reveal robustness and an accurate identification of the sequence of the multiple faults. We remark also some false alarms during the transient

period of the fault injection within the windows [50,100], [150,200]. These false alarms occur due to the fact that the IMM_UKF algorithm is based on the steady-state residual measurements.

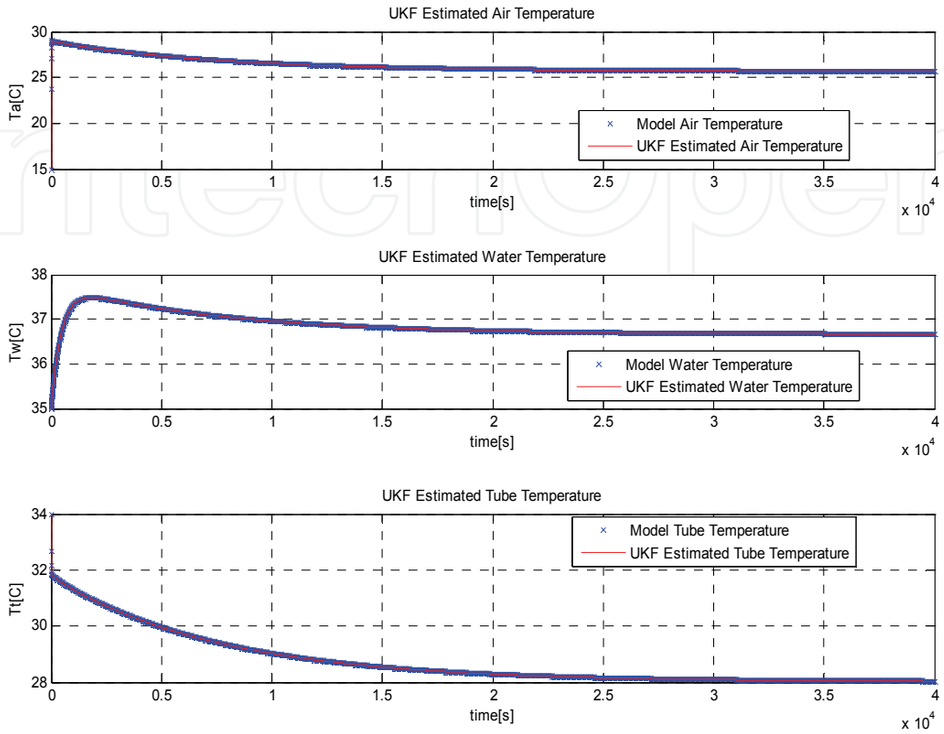

Fig. 8. The UKF state estimation with the same initial conditions with the process model

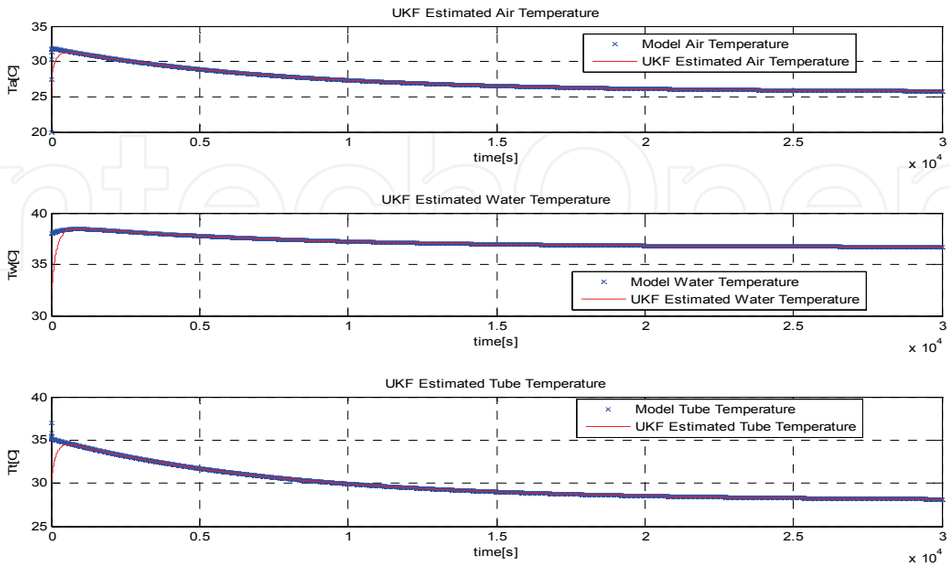

Fig. 9. The UKF state estimation with different initial conditions than the process model

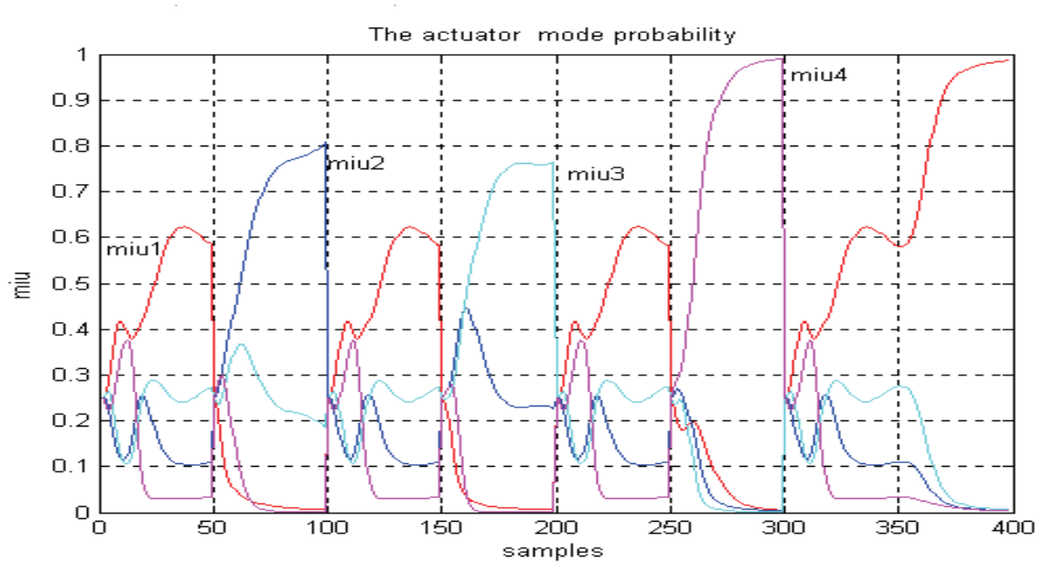

Fig. 10. The evolution of the mode probability for the sequence
$z = [z_1\ z_2\ z_1\ z_3\ z_1\ z_4\ z_1], u = [u_1\ u_2\ u_1\ u_3\ u_1 u_4\ u_1]$

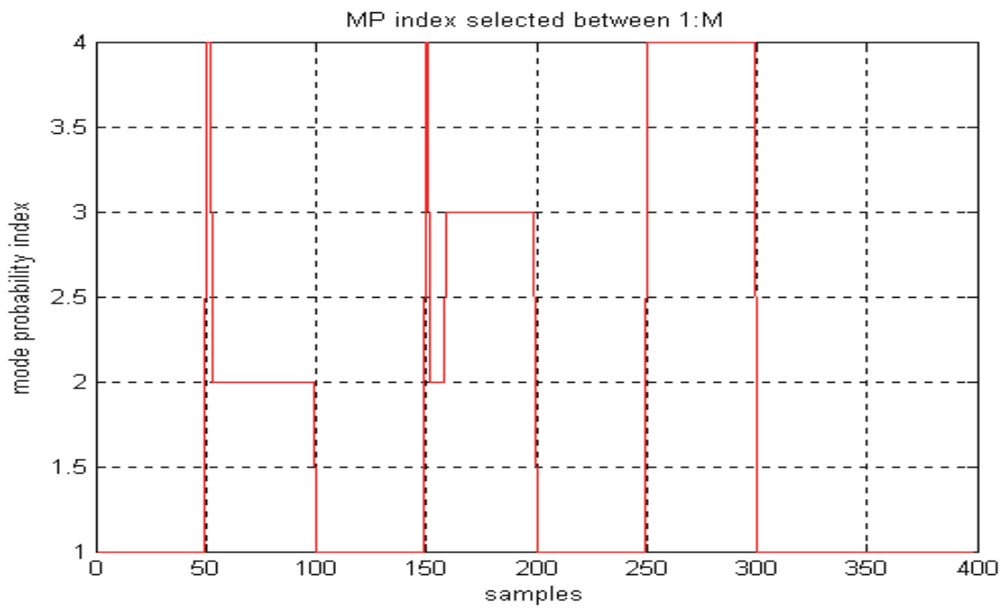

Fig. 11. The index of the mode probability for the sequence
$z = [z_1\ z_2\ z_1\ z_3\ z_1\ z_4\ z_1], u = [u_1\ u_2\ u_1\ u_3\ u_1 u_4\ u_1]$

6. Conclusion

In this paper, we present two fault detection model-based approaches, namely frequency analysis and an Interactive Multiple Model based on Unscented Kalman Filter (IMM_UKF)

state estimation. The frequency analysis method is simple and practical, but not accurate and robust. The results of IMM_UKF algorithm obtained in simulation environment reveal the superiority of this algorithm compare to frequency analysis approach. The IMM_UKF algorithm is more accurate and capable to estimate the dynamic evolution of the state variables for monitoring purposes in HVAC systems. The IMMM_UKF algorithm is faster and eliminates completely the linearization of the process dynamics. Also the robustness to the measurement and process noises as well as parameter changes is a further benefit of this algorithm. Also the superiority of the UKF algorithm is well documented in the literature [Haykin, 2003; Joseph, 2003; Tudoroiu et al., 2006]. However the gain of the UKF algorithm is for nonlinear cases, but sometimes it is very difficult to obtain the analytical model of the nonlinear system. Based on these results we will be capable to identify the degradation level of the faulty valve. The approach is probabilistic and gives results more accurate than the spectral analysis. The results obtained are encouraging and the performance of the IMM_UKF algorithm will be tested. The recovery mode development to complete the IMM_UKF algorithm in order to avoid the degrading in performance of the closed-loop HVAC systems during the failures periods will be explored in the future work. In our research, we have studied the possibility of using two interacting multiple models based on extended (IMM_EKF) and unscented (IMM_UKF) Kalman Filter estimation techniques for detection and diagnosis of faults in reaction wheels of the attitude control system (ACS) in a satellite and the valve actuators of HVAC systems. The main contributions are summarized briefly as follows:

a. Detection and identification of reaction wheel faults of the ACS and HVAC systems due to a number of possible sources that generate soft and hard anomalies during a scientific mission of a satellite or valve operation.
b. Implementation of a bank of parallel Kalman filters for faulty modes covering a rather broad set of the most likely and commonly possible scenarios of reaction wheel and valve actuators failures,
c. Detection and diagnosis of both partial and significant reaction wheel and valve actuators failures for different scenarios using the IMM_EKF and IMM_UKF estimation algorithms,
d. Comparison of performance capabilities and advantages of IMM_ UKF estimation algorithm with respect to the IMM_EKF estimation algorithm, and
e. Robustness analysis of both the IMM_EKF and IMM_UKF estimation algorithms to the selection of model transition probabilities, modeling errors, and noise statistics under different scenarios.

The approach proposed in this paper is probabilistic in nature and yields results that are more accurate and having good fault classification capabilities than the spectral analysis that are well studied in the literature [Tornhill et al., 2001; Tudoroiu & Zaheeruddin, 2005]. Based on fault identification analysis that is carried out it can be observed that the IMM_UKF estimation algorithm is robust to modeling uncertainties, and to statistics of noise measurements and process noise. Our proposed algorithms work similar to a neural network estimator and classifier that is described in e.g. [Li, 2005; Sobhani, 2006] where dynamic neural network architectures are employed to perform satisfactory FDDI. Compared to a neural network estimator and classifier, IMM_UKF estimation algorithm doesn't need an on-line training that takes an extensive amount of computational

resources. Another similar approach uses observer banks of autoregressive time series models for fault diagnosis, based on Box-Jenkins linear autoregressive models, back-propagation neural networks, and radial function networks. Compared to the above approaches and IMM_EKF estimation algorithm, the IMM_UKF estimation algorithm performs better and has a much less computational burden and complexity, and it furthermore operates much faster. Perhaps the biggest drawback of predictive model-based approaches is the need for a suitable quantity of data for training and testing the system during the development phase. Moreover, stability of the IMM_UKF estimation algorithm still remains an open question, which needs further investigation. Also, the behavior of the IMM_UKF estimation algorithm for diagnosis in a fast or rapidly changing process dynamics needs to be explored further.

7. References

Bialke B. (1998). High Fidelity Mathematical Modeling of Reaction Wheel Performance, *Advances in the Astronautical Sciences*, pp. 483-496, 1998.

Haykin S. (2003). *Adaptive filter theory - Fourth edition*, Prentice Hall, 2003.

Joseph, LaViola Jr. (2003). A Comparison of Unscented and Extended Kalman Filtering forEstimating Quaternion Motion, *Proceedings of the American Control Conference* Denver, Colorado June 4-6, 2003.

Julier S. J., Uhlman J.K. (1997). A New Extension of the Kalman Filter to Nonlinear Systems, *Proceedings of Aero Sense, the 11th International Symposium on Aerospace/Defense Sensing, Simulation and Controls*, 1997, pp.182-193.

Li Z., Ma L. & Khorasani K. (2005). Fault Detection in Reaction Wheel of a Satellite using Observer-based Dynamic Neural Networks, *Proceedings of International Symposium on Neural Networks*, May 2005.

Plett G. (2004). Extended Kalman filtering for battery management systems of LiPB-based HEV battery packs - Part 3. State and parameter estimation, *J. Power Source.*, 134, no. 2,pp. 277-292, 2004.

Mihaylova L. & E. Semerdjiev E. (1999). An Interacting Multiple Model Algorithm for Stochastic Systems Control, *Information and Security*, Vol. 2, 1999.

Mihaylova L. & E. Semerdjiev E. (1999). Interacting Multiple Model Algorithm for Maneuvering Ship Tracking Based on New Ship Models, *Information and Security*, Vol. 2, 1999.

Semerdjiev E. & Mihaylova L. (1998). Variable and Fixed Structure Augmented InteractingMultiple Model Algorithms for Maneuvering Ship Tracking Based on New Ship Models, *Bulgarian Academy of Sciences, Central laboratory for Parallel processing*, Report, 1998.

Sobhani E., K. Khorasani K. & Tafazoli S. (2005). Dynamic Neural Network-based Estimatorfor Fault Diagnosis in Reaction Wheel Actuator of Satellite Attitude Control System, *Proceedings of the 2005 International Joint Conference on Neural Networks*, August 2005.

Thornhill N.F., Shah S.L. & Huang B. (2001). Detection of Distribution Oscillations andRoot-Cause Diagnosis, *Proceedings of the IFAC Workshop on on-line Fault*

Detection and Supervision in the chemical process industries, Korea, pp. 167-172, June 2001.

Tudoroiu N., Zaheeruddin M. (2004). Fault Detection and Diagnosis of the ValveActuators In HVAC Systems Using Interactive Parallel Kalman Filters Bank, *Proceedings of the 29th Annual Congress of the American Romanian Academy of Arts and Sciences (ARA)*, Bochum, Germany, September 7-12, 2004, pp 395-398.

Tudoroiu N., Zaheeruddin M. (2005). Frequency Analysis Approach to Detect and Diagnosis Faults in Discharge Air Temperature (DAT) Systems, *Proceedings of the 30th Annual ARA Congress,* July 5-10, 2005, Chisinau, Republic of Moldova, pp.597-600.

Tudoroiu N., Zaheeruddin M. (2005). Fault Detection and Diagnosis of Valve Actuators in HVAC Systems, *Proceeding of the 2005 IEEE International Conference on Control Applications*, August 29-31, 2005, Toronto, Canada, ISBN:0- 7803-9354-6.

Tudoroiu N., Khorasani K. (2005). State estimation of the Vinyl Acetate Reactor using Unscented Kalman Filters (UKF), *2005 International Conference on Industrial electronics and Control Applications, ICIECA 2005*, Quito, IEEE, ISBN :0-7803-9420-8.

Tudoroiu N., Zaheeruddin M. (2006). Fault Detection and Diagnosis of Valve Actuators in Discharge Air Temperature (DAT) Systems, using Interactive Unscented Kalman Filter Estimation, *International Symposium on Industrial Electronics, ISIE2006*, 9-13 July 2006, Montreal.

Tudoroiu N., Sobhani-Tehrani E. & Khorasani K. (2006). Interactive Bank of Unscented Kalman Filters for Fault Detection and Isolation in Reaction Wheel Actuators of Satellite Attitude Control System, *IECON'2006, Paris, 32nd Annual Conference of the IEEE Industrial Electronics Society*, November 2006.

Tudoroiu N. & Khorasani K. (2007). Satellite Fault Diagnosis using a Bank of Interacting Kalman Filters, *IEEE Transactions on Aerospace and Electronic Systems*, Vol. 43, No.4, October 2007, ISSN 0018-9251, pp.1334-1350.

Narendra K. & Balakrishnan J. (1997). Adaptive Control Using Multiple Models, *IEEE Transaction on Automatic Control*, Vol. 42, N0.2, pp.171-187, 1997.

R. J. Patton R.J., Frank P.M. & Clark R. N. (1989), *Fault Diagnosis in Dynamic Systems, Theory and Applications*, Englewood Cliffs, NJ: Prentice Hall, 1989.

Zaheeruddin M., Patel R. V. (1995), Optimal Tracking Control of Multi Zone Indoor Environnemental Space, *ASME Journal Dynamic Systems, Measurement and Control*, Vol. 117, pp. 292-303, 1995.

Zhang Y., & Xiao Rong-Li. (1997). Detection and Diagnosis of Sensor and Actuator Failures using interacting multiple-model estimator, *Proceedings of the 36th IEEE Conference on Decision and Control*, pp. 4475-4480, San Diego, CA, Dec. 1997.

Zhang Y., & Xiao Rong-Li. (1998). Detection and Diagnosis of Sensor and Actuator Failures using IMM Estimator, *IEEE Transaction On Aerospace and Electronic Systems*, Vol.34, No.4, pp. 1293-1311, October 1998.

Wan E. A, Merwe R. (2000). The Unscented Kalman Filter for Nonlinear Estimation, *Proceedings IEEE Symposium 2000 (AS-SPCC)*, Lake Louise, Alberta, Canada, Oct. 2000.

Kalman Filter Recent Advances and Applications

Edited by Victor M. Moreno and Alberto Pigazo

ISBN 978-953-307-000-1
Hard cover, 584 pages
Publisher InTech
Published online 01, April, 2009
Published in print edition April, 2009

The aim of this book is to provide an overview of recent developments in Kalman filter theory and their applications in engineering and scientific fields. The book is divided into 24 chapters and organized in five blocks corresponding to recent advances in Kalman filtering theory, applications in medical and biological sciences, tracking and positioning systems, electrical engineering and, finally, industrial processes and communication networks.

How to reference

In order to correctly reference this scholarly work, feel free to copy and paste the following:

Nicolae Tudoroiu, Kash Khorasani, Mohammed Zaheeruddin, Eshan, Sobhani-Tehrani, Dumitru Burdescu and Elena-Roxana Tudoroiu (2009). Application of the Unscented Kalman Filter (UKF) Estimation Techniques for Fault Detection Diagnosis and Isolation (FDDI) in Attitude Control (AC) and Heating Ventilation Air Conditioning (HVAC) Systems, Kalman Filter Recent Advances and Applications, Victor M. Moreno and Alberto Pigazo (Ed.), ISBN: 978-953-307-000-1, InTech, Available from: http://www.intechopen.com/books/kalman_filter_recent_adavnces_and_applications/application_of_the_unscented_kalman_filter__ukf__estimation_techniques_for_fault_detection_diagnosis

INTECH
open science | open minds

InTech Europe
University Campus STeP Ri
Slavka Krautzeka 83/A
51000 Rijeka, Croatia
Phone: +385 (51) 770 447
Fax: +385 (51) 686 166
www.intechopen.com

InTech China
Unit 405, Office Block, Hotel Equatorial Shanghai
No.65, Yan An Road (West), Shanghai, 200040, China
中国上海市延安西路65号上海国际贵都大饭店办公楼405单元
Phone: +86-21-62489820
Fax: +86-21-62489821

IntechOpen